

# 3D reconstruction of road surfaces using an integrated multi-sensory approach

Si-Jie Yu\*, Sreenivas R. Sukumar, Andreas F. Koschan, David L. Page, Mongi A. Abidi

*Imaging, Robotics, and Intelligent Systems Laboratory, Department of Electrical & Computer Engineering,  
The University of Tennessee, Knoxville, TN 37996, USA*

Received 15 February 2006; received in revised form 20 September 2006; accepted 8 December 2006  
Available online 15 February 2007

---

## Abstract

In this paper, we present our experience in building a mobile imaging system that incorporates multi-modality sensors for road surface mapping and inspection applications. Our proposed system leverages 3D laser-range sensors, video cameras, global positioning systems (GPS) and inertial measurement units (IMU) towards the generation of photo-realistic, geometrically accurate, geo-referenced 3D models of road surfaces. Based on our summary of the state-of-the-art systems for a road distress survey, we identify several challenges in the real-time deployment, integration and visualization of the multi-sensor data. Then, we present our data acquisition and processing algorithms as a novel two-stage automation procedure that can meet the accuracy requirements with real-time performance. We provide algorithms for 3D surface reconstruction to process the raw data and deliver detail preserving 3D models that possess accurate depth information for characterization and visualization of cracks as a significant improvement over contemporary commercial video-based vision systems.

© 2007 Elsevier Ltd. All rights reserved.

*Keywords:* Road surface reconstruction; Multi-sensor integration; 3D geometric mapping; Laser range scanning

---

## 1. Introduction

Every year a substantial amount of maintenance costs occur for collecting and evaluating road distress data. The inspection procedure that involves personnel walking or driving slowly over asphalt and concrete pavements and subsequently observing surface defects and degradation, is not only cumbersome and time consuming, but is also susceptible to human subjectivity, error, and inefficiency. With the safety of the personnel and the passengers that use the roadways in mind, this functional and important process of inspection can be significantly improved using a formalized imaging system. Several companies have hence worked towards the production of automatic commercial inspection systems to meet the specific requirements in

assessing distress on the road surfaces using video cameras and image processing algorithms. With limited success using the 2D image-based systems, and with the advent of 3D laser scanners, the next logical improvement appears to be the use of accurate 3D maps for road distress analysis.

Towards that end, we propose a mobile laser scanning approach to acquire 3D data and implement surface reconstruction techniques to create 3D geometric models. The output 3D models from our two-stage acquisition and processing methodology brings together 3D laser scanning from the field of optics and surface reconstruction techniques from computer vision and graphics research areas into the engineering for road distress inspection. Though our experiments with a simple prototype in this paper are targeted towards road surface mapping, our approach should impact inspection work for airport runways and highways with minor modifications like deploying high-speed laser scanners. The detailed geo-referenced road surface models from our system can also be used to enrich available 3D databases embedded in geographical information systems (GIS). In describing such

---

\*Corresponding author. Tel.: +1 865 235 4052.

E-mail address: [yu.sijie@gmail.com](mailto:yu.sijie@gmail.com) (S.J. Yu).

a system and processing pipeline, we list the following two contributions of this paper:

- *Multi-sensor integration for road surface mapping:* We propose an integrated multi-sensor approach for efficiently and automatically capturing 3D road surface data and demonstrate the methods involved using a prototype data acquisition system.
- *Multi-stage processing system:* We list a set of processing algorithms, which combine methods from computer vision and computer graphics for creating coarse models as a precursor to constructing detailed piecewise smooth surfaces from scattered point cloud data. The coarse model is obtained by first gridding and interpolating the data, while the detailed model is the output after smoothing and denoising using algorithms that preserve sharp features and geometric details.

We have organized this paper to emphasize the above contributions in the construction of a multi-modal integrated imaging system that is capable of real-time data collection and processing. In Section 2, we summarize existing commercial systems targeting road surface inspection. The literature survey emphasizes the design methods implemented thus far and also serves as a reference to understand the difficulty in building systems for real-time deployment. We introduce our prototype system and explain the idea behind using multi-modal sensors in Section 3. After explaining data acquisition, we discuss the integration and processing algorithms on the multi-modality data. The integration involves the representation and reconstruction of range data into a spatially meaningful visualizable form using the information from position and orientation sensors. We show the 3D models generated using our system driving a van along a test area containing different types of cracks in Section 4 and conclude with recommendations for possible improvements and reproducibility of our system in Section 5.

## 2. Related work

The key to successful road surface evaluation lies in identifying different types of distress and linking them to the cause. In particular, the interest in standard practice is on cracks and debris as dominant distress data [1]. Targeting such a goal of being able to detect road distress, the most popular method for automatically acquiring road data is through digital imaging using vision cameras. Some examples of commercial imaging systems include Pathview [2], ARAN [3], and Digital Imaging System [4]. As a significant next step using digital cameras, video logging is also adopted as a common technique in storing and processing continuous image data. VIASAT [5], GeoVAN [6], and L.C.P.C [7] are some recent commercial systems that are based on video logging. The common feature between these commercial systems is that one or more cameras are mounted along with archival equipment for

recording 2D images of the road surface. Another configuration requires the placement of two cameras separated by a baseline distance to acquire stereo images. From the two stereo images and with the calibration information of the cameras, 3D information is estimated using epipolar geometry. However, the accuracy from 3D reconstruction has not been sufficient for distress analysis. In addition to multiple cameras, some of these systems like GPS Vision [8] use position sensors such as the GPS for global location information. The integration of GPS information with the video to create GIS-like databases of road surfaces claims to improve road network identification and pavement inspection for better maintenance and data management. Part of the success for these imaging-based systems can be attributed to the ease of using the acquired images and processing them to analyze distress information, such as crack patterns, width, length, counts, areas, and in some cases even depth [9].

One major issue with pure video-based systems is their inability to discriminate dark areas not caused by pavement distress such as tire marks, oil spills, shadows, and recent fillings [10]. Moreover, the 3D geometric information, in particular the depth, is difficult to derive from 2D images at the required scale of accuracy. Shadows and poor illumination are also major problems for daytime operation though they can be overcome using additional lighting systems or by acquiring data in the night after sunset [11].

The introduction of laser scanning techniques is only a recent trend in support of the image-based techniques. The advantage of using laser scanners is that the 3D information of the road surface acquired at high speed can aid in detecting cracks that were not detected by traditional imaging approaches. The maps produced by DistressVIEW 3D [12] representing the left and right ruts in a 2D color image is an example of 3D sensors that support the image data.

We briefly explain some 3D methods used for road surface reconstruction before presenting our system in Section 3. Javidi et al. [13] have proposed a phase shifting digital interferometry-based technique as an improvement for ARAN [3] towards measuring 3D depth. The basic principle behind using interferometry is to project multiple laser beams to a CCD camera and then observe the diffraction patterns to reconstruct 3D coordinates using holography. Though their system is able to derive crack depth and integrate with 2D images, the system is too sensitive to the vibrations of a moving van. Laurent et al. introduced a multi-scanner synchronized system for measuring dense 3D coordinates [14]. This system is efficient when mounted on a mobile vehicle driving at high speed and is able to output a binary image with 255 (bright) denoting non-distress areas and zero (dark) denoting distress areas in near real time. Bursanescu [15] introduced a similar system consisting of six sensors for high-speed and high-resolution scanning. Their system outputs binary crack maps along with longitudinal road parameters. Abuhadrous [16] also scans road surfaces together with

various spatial objects like traffic signs, trees and vegetation in the field of view. The processing methods in his system extract range points belonging to road edges and centers, and then model the road surfaces using feature triangulation. Abuhadrous's system produces road models that can indicate curves in the roads and hilliness of the terrain, but it cannot recover geometric details of surface distress.

Tao has summarized road data-capturing methods using both 2D and 3D techniques in his comprehensive survey. We direct the reader to his list of commercial road data acquisition systems in the United States for further information [17]. From his survey and our own study of several published methods, we identify the shortcoming of these systems to deliver visualizable detailed geometry combined with topology information of road surfaces. Moreover, some 3D laser-based systems require blocking traffic when acquiring data because of the slow acquisition and processing speed with their equipment and processing methods. Our system is capable of high-speed acquisition and our choice of processing methods that we will explain in the following section substantially reduces the time between acquisition and analysis in overcoming several shortcomings with the state of the art.

### 3. The mobile laser scanning and surface reconstruction approach

In this section, we explain the implementation details of our proposed approach along the two contributions of the multi-sensor integration and post processing system summarized in the introduction in Section 1. We will begin with multi-sensor integration for the mobile mapping system (MMS), which is essentially a van equipped with laser scanners, video cameras, GPS, orientation sensors, and computer processing equipment. The basic idea behind using multi-modality sensors is to collect different kinds of information from the physical environment for better accuracy and resolution. Our acquisition software interfaces with the hardware to time stamp and simultaneously record multi-sensor data to a computer, which is also a part of the mapping system. Our software is able to obtain

multi-sensory data in an efficient archival mode for long durations of time (typically, 20–30 min). In the second stage of processing, a set of algorithms are applied to the acquired data to reconstruct 3D road surfaces. The algorithms that we explain later in this section are selected to deal with measurement noise, outliers, missing data, along with sharp crack features. Our approach is illustrated in Fig. 1, which depicts the main processing steps involved starting from building the system to acquire real data leading up to the detailed 3D surface reconstruction.

#### 3.1. Data acquisition system

Our data acquisition system includes an instrumented van with rigidly mounted sensors. The sensors in our prototype include a SICK LMS 200 laser scanner, a Leica GPS System 500, a Xsens MT9 inertial measurement unit, and a Sony DCR-TRV730 Digital Camcorder video camera. The data acquired with the SICK scanner represents 3D range values containing the crack information while position and orientation information from the GPS and IMU is used for spatial visualization. The images from the video camera can be used for texturing the 3D models as another processing step.

The differential GPS system that we use delivers data at 10 Hz with 2 cm positional accuracy. With road surfaces being our interest, the laser scanning system is configured to be downward looking along with other equipment mounted on a rigid flat metal plate. The rigid arrangement of sensors helps in establishing the relationship between the local coordinate frames of each sensor. Data integration then becomes the process of aligning multi-sensory data into a common global reference frame using different transformation functions. We choose the GPS coordinate frame as global 3D position reference and IMU Euler angle measurements for 3D orientations about that reference to compensate for the roll, pitch, and yaw changes due to vehicle motion. Fig. 2 shows the instrumented van with sensors mounted. The top inset in the figure shows the IMU and the GPS system while the bottom inset shows the SICK laser scanner hanging out of the same rigid metal frame.

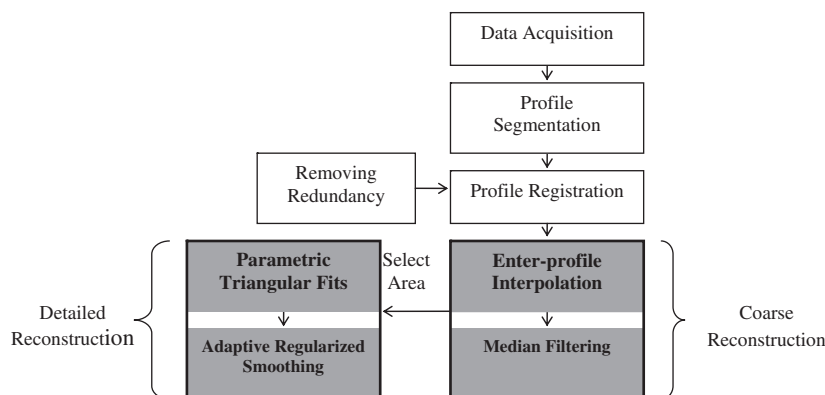


Fig. 1. Block diagram of the proposed processing pipeline starting from the construction of the acquisition system up to 3D reconstructed surface models.



Fig. 2. The proposed prototype mobile mapping system consists of a vehicle, a range scanner, a GPS, an IMU, and a video camera.

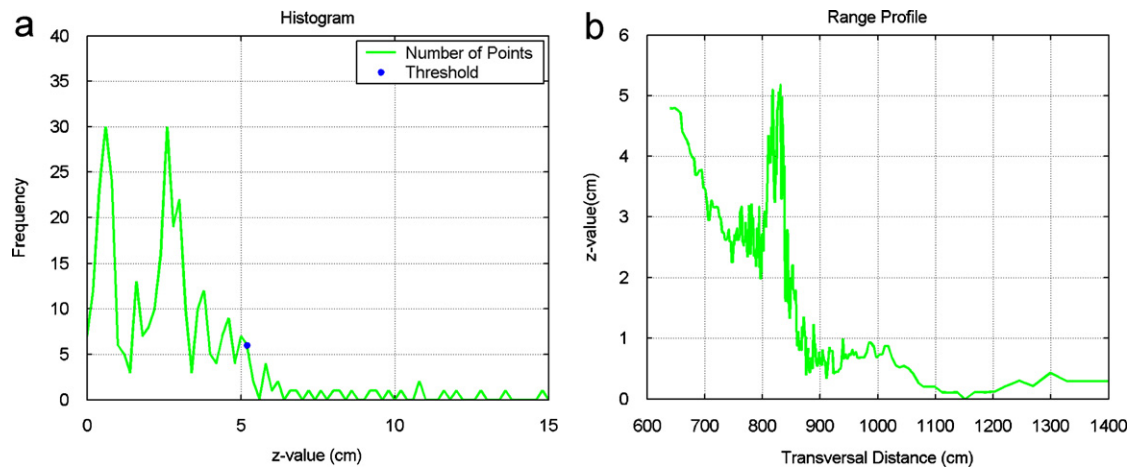


Fig. 3. Profile segmentation. (a) Find the peak  $N$  and then search for  $N/2$  which is the threshold value; (b) Range points filtered by the threshold value (i.e. 6.3 cm) estimated from (a).

### 3.2. Postprocessing

We utilize a set of postprocessing algorithms to create geometrical 3D models of road surfaces with a relatively higher accuracy when compared to competing methods. This stage intends to introduce recent 3D techniques to the pipeline of large-scale modeling and to cope with imperfections inherent in the outdoor scanning process. A simple example of an imperfection associated with the equipment is the random measurement noise. Even if we ignore the effects of dynamic motion and dynamic environments, the GPS stationary measurements within 5 min could generate root-mean square (RMS) errors of 2.0, 2.3, and 3.5 cm along directions of in Cartesian earth coordinates [18]. The 3D scanner also is noisy to the extent that in scanning a flat

indoor concrete surface, the measurement RMS error of 8000 profiles can be 0.6 cm [18].

#### 3.2.1. Profile segmentation

Our range scanner samples line profiles 8.0 m on either side of the motion direction. Hence each profile has points pertaining to road surfaces and points pertaining to objects beyond the road such as trees, cars, or curbs within the scanning range. We segment the profiles to ignore points belonging to surfaces from those objects that are not our interest in mapping. By construction of the scanning apparatus, most of the range points should belong to road surface and have similar depth ( $z$ ) values. Therefore, the  $z$ -value histogram of each profile should have a peak discriminating non-surface and surface points as seen in

Fig. 3(a). We execute the following three-step algorithm [19] for each profile to select only the points that are samples of the road surface:

- (1) Determine a threshold value:
  - (i) Select the bin with the highest frequency value and take as  $N$ ; (ii) Search the bin  $N1$  with at least 40% of number of data points of bin  $N$ ; (iii) Search the bin  $N2$  with at least 40% of number of data points of bin  $N1$  and take  $N2$  as the threshold value.
- (2) Filter those points with local  $z$  values larger than the threshold value;
- (3) Further filter scattered points reflected from objects on surfaces and points with small normal angles between scanning plane and laser. The filtering conditions can be described as (i) second derivatives are larger compared with neighboring points and as (ii) angles between scanning surface and scanner beam are smaller than a predefined value.

This procedure essentially filters out unnecessary data obtained from the laser scanners where the data are not our interest. This step is an important pre-processing step before we can execute surface reconstruction algorithms from 3D scattered point cloud data. Fig. 3(b) shows a segmented profile using a threshold value obtained from its histogram shown in Fig. 3(a).

### 3.2.2. Profile registration

With the van along with the sensors and software programs archiving data continuously, we accumulate range profiles along with position and orientation information. We align these profiles to a point cloud for maintaining the topology of the road surface and also to compensate for the vibrations in motion. The profile registration is a spatial transformation incorporating translation and rotation between successive profiles. The transformation matrix for dynamic motion on roads involves six degrees of freedom (DoF), three for the GPS position and three for the IMU orientations. If an assumption about the planarity and smoothness of the road surfaces can be made then only considering three DoF is sufficient [20].

Theoretically, the profile registration procedure begins with the definition of a global coordinate system  $(X, Y, Z)$ . We choose the GPS frame as the global reference frame, with two axes along the earth surface and the third one indicating the height about the earth surface. Then the registration transformation is applied to each profile for transforming the measurements from the range sensor local coordinates to the global coordinates. The transformation is formulated as shown below [21]. We note that the position sensors cannot provide the same degree of accuracy as the range measurements, which can become a problem when the accuracy from the GPS system falls below acceptable levels. In the latter case, additional information can be derived from the video sequence for

localization [22].

$$(X, Y, Z)^T = T_{\text{hg}} T_{\text{lg}}(0, y, z)^T,$$

$$T_{\text{hg}} = T_{\text{gps}} R_{\text{imu}},$$

where  $(0, y, z)^T$  is the coordinates measured by scanner, and  $T_{\text{lg}}$  is the translation from scanner to GPS, which is manually measured from the rigid configuration.  $T_{\text{gps}}$  and  $R_{\text{imu}}$  are GPS and IMU measurement matrices, respectively. They are combined to generate the pose matrix  $T_{\text{hg}}$ . Usually the scans are gathered sequentially to describe a surface in a temporal order, but when the van turns a large heading angle, we can occasionally obtain overlapping points digitizing the same road surface and thus generating redundancy. Hence, each range measurement  $r$  is processed through the filter that we describe below. This filtering procedure draws inspiration from [23],

$$\text{RF}(r) = \begin{cases} \text{keep,} & r \cos \theta \leq d_{\text{crit}} \\ \text{remove,} & \text{otherwise} \end{cases}, \quad (3)$$

where  $d_{\text{crit}} = \Delta s / \sin(\Delta \theta)$ ,  $\Delta s$  is the arc length between successive points and  $\Delta \theta$  is equal to the angular scanning resolution (e.g.  $0.5^\circ$ ).

### 3.2.3. 3D surface reconstruction

The result after registering range points is non-uniformly and irregularly distributed. Furthermore, with water puddles or glass objects on the road surface at the time of scanning, range data may be missing in these areas. Our solution for visualizing scattered point clouds of road surface data is to first grid the surface using interpolation methods and then fill holes in areas missing range measurements. We perform cubic spline interpolation within the scattered points in a single profile. Considering the large amount of raw data that we need to process, it is not practical with our resources to perform 2D or 3D grid methods in real time. After interpolation, a median filter ( $3 \times 3$ ) is applied to remove sensor impulse noise. The interpolated points are then triangulated and rendered. We note that this gridding and interpolation is on individual profiles and not on the entire surface. We call this process of generating a 3D point cloud as coarse surface reconstruction. By observing the coarse models, and looking at the variation of 3D depth measurements, cracks in smaller regions can be identified. These are points of interest in our application and they are selected for further processing.

We use another set of algorithms to reconstruct a detailed surface from selected points of interest. This processing stage is designed to handle problems such as noise and measurement outliers while at the same time to preserve sharp features that may correspond to road distress. Also, this stage considers the underlying surface instead of the profiles as in the previous stage of interpolation. We have chosen a parametric triangular interpolation scheme [24] for detail reconstruction of road

surfaces. The motivation for choosing triangular interpolation arises from the capability of the interpolation method to represent arbitrary topological types and at the same time maintaining the continuity and smoothness across connected patches. Since the parametric scattered data interpolation scheme mainly focuses on truthful recovery of topology from possibly incomplete data sets, we have to be cautious in not violating the assumptions of relaxed continuity [25].

The motivation for the next processing step aims at removing impulse noise and outliers introduced during the grid assignment and interpolation process [26]. We use a median filter for Gaussian distributed noise in the reconstructed point cloud [27]. A median filter is a smoothing operation and we hence need to be careful in smoothing small discontinuities in the coarse surface that might be important for detecting road distress. A detail-preserving median filter is hence applied to especially target these issues. In the next paragraphs we explain the gridding and Clough–Tochler interpolation procedure on the coarsely reconstructed model that delivers 3D geometric models of high detail using a detail-preserving smoothing algorithm.

*Parametric triangular interpolation:* The Clough–Tocher method [28] is a standard technique for parametric triangular interpolation that Foley and Opitz [29] have improved by adding cross-boundary conditions. Mann [30] combines the Clough–Tocher method with the enhancements, suggested by Foley and Opitz, to yield cubic precision while maintaining continuity. Our scheme is based on Mann’s work with the improvement of estimating boundary control points using vertices and their normals. Our purpose is to reconstruct accurate surface information from the scattered coarse point cloud data. We are inspired by the work of Saaban [31] to construct local quadratic polynomials to compute surface normals, and further to use a popular 2D Delaunay triangulation method for surface reconstruction. We explain this interpolation scheme in the following paragraphs.

Consider a cubic triangular Bézier patch  $P$  of the form

$$\begin{aligned} P(u, v, w) = & p_{300}u^3 + 3p_{210}u^2v + 3p_{120}uv^2 + p_{030}v^3 \\ & + 3p_{021}v^2w + 3p_{012}vw^2 + p_{003}w^3 + 3p_{102}uw^2 \\ & + 3p_{201}u^2w + 6p_{111}uvw, \end{aligned} \quad (4)$$

where  $u$ ,  $v$  and  $w$  are barycentric coordinates of a point inside the triangular patch. The values  $p_{ijk}$ ,  $i, j, k = \{0, 1, 2, 3\}$  are  $z$ -values of ten Bézier control points defined on the triangular patch. Note that  $p_{300}$ ,  $p_{030}$ , and  $p_{003}$  are actually three vertices of the triangle and  $p_{ijk}$ ,  $i \neq j \neq k$ ,  $i, j, k = \{0, 1, 2\}$  are six key control points from which the remaining controls points can be derived. A more accurate method is used to estimate key control point values using both vertices and normals, rather than using information at the vertex alone.

Considering  $V_1(x_1, y_1)$ ,  $V_2(x_2, y_2)$  and  $V_3(x_3, y_3)$  as the three vertices in the barycentric coordinate space defined by axes  $(1, 0, 0)$ ,  $(0, 1, 0)$  and  $(0, 0, 1)$ , we can define a quadratic polynomial function  $F(x, y) = a_1x^2 + a_2xy +$

$a_3y^2 + a_4x + a_5y + a_6$  to approximate  $z$ -value for each vertex. The partial derivatives of  $F$ , evaluated at a vertex in the underlying grid (e.g.  $V_1$   $F_x(x_1, y_1)$ , and  $F_y(x_1, y_1)$ ), can be computed with the equations shown below

$$F_x(x_1, y_1) = 2a_1x_1 + a_2y_1 + a_4, \quad (5)$$

$$F_y(x_1, y_1) = a_2x_1 + 2a_3y_1 + a_5. \quad (6)$$

The neighboring triangle vertices and the ordinary least squares procedure is used to solve for parameters  $a_1, a_2, a_3, a_4, a_5, a_6$ . Then, using the definition of  $e_{12} = (-1, 1, 0)$  representing the directional edge connecting  $V_1$  and  $V_2$ , the directional derivative along  $e_{12}$  at  $V_1$  is computed as shown below

$$\begin{aligned} D_{e_{12}}P(1, 0, 0) &= \left( \frac{\partial x}{\partial v} - \frac{\partial x}{\partial u} \right) F_x(x_1, y_1) + \left( \frac{\partial y}{\partial v} - \frac{\partial y}{\partial u} \right) F_y(x_1, y_1) \\ &= (x_2 - x_1)F_x(x_1, y_1) + (y_2 - y_1)F_y(x_1, y_1). \end{aligned} \quad (7)$$

The right hand of (7) can be computed from (5) and (6). Considering (4), we can also obtain,

$$D_{e_{12}}P(1, 0, 0) = \frac{\partial P(1, 0, 0)}{\partial v} - \frac{\partial P(1, 0, 0)}{\partial u} = -3(p_{300} - p_{210}). \quad (8)$$

The (8) can be reformulated as (9) to compute the coefficient  $p_{210}$

$$p_{210} = \frac{1}{3}D_{e_{12}}P(1, 0, 0) + p_{300}. \quad (9)$$

The other  $p_{ijk}$ ,  $i \neq j \neq k$ ,  $i, j, k = \{0, 1, 2\}$  values are computed in a similar fashion. (See Mann [30] for a more detailed explanation of the computation procedure.)

*Adaptive regularized smoothing:* So far, using the Clough–Tocher interpolation we have interpolated the scattered coarsely reconstructed data into a dense grid  $P$ . During the interpolation, our experience indicates that noise is also amplified. To reduce the impact of noise, outliers, and discontinuities, we employ a regularized smoothing algorithm that effectively reduces the Gaussian and impulse noise while preserving discontinuities and edges [32]. The formulation of this algorithm is based on the following regularization function

$$\begin{aligned} \hat{F} = \arg \min_F & \left( \|F - P\|^2 + \lambda_C \sum_{i=1}^{N_I} \|I_i C_i F\|^2 \right. \\ & \left. + \lambda_M \|F - P_M\|^2 \right) \end{aligned} \quad (10)$$

where  $C_i$  refers to local Laplacian filters,  $P_M$  is the median filtered result of  $P$ , and  $\lambda_C$ ,  $\lambda_M$  are regularization parameters. In some sense, Eq. (10) can be thought of as a formulation of an “energy function” incorporating a median filter constraint for removing noise and high-pass filter constraints for suppressing local high frequency components. To find a solution for Eq. (10), we equate the gradient of  $F$  to zero, and converge to an iterative

solution. At the  $l$ th ( $l = 0, \dots, L_s$ ) iteration, the detail-preserving smoothed results can be expressed as

$$F_l = \begin{cases} \beta G, l = 0 \\ F_{l-1} + \beta \left[ P + \lambda_M P_M - \left( \lambda_C \sum_{i=1}^N I_i C_i^T C_i \right) \circ F_{l-1}, L_s \geq l > 0 \right] \end{cases} \quad (11)$$

where  $\beta$  is a convergence parameter that controls the number of iterations  $L_s$ . The convergence criterion that we set is based on the term  $\|F_l - F_{l-1}\|/N$  iterating below a predefined threshold. In our implementation, we convolve  $C_i$  with the previous estimate of  $F_{l-1}$  at each iteration. For slightly better results, we also define five morphological filters, other than Laplacian filters, to detect high-frequency components along vertical, horizontal,  $45^\circ$  and  $135^\circ$  directions in a robust fashion. These filters are listed below

$$C_1 = \frac{1}{12} \begin{bmatrix} 0 & 0 & -1 & 0 & 0 \\ 0 & 0 & -1 & 0 & 0 \\ 0 & -1 & 6 & -1 & 0 \\ 0 & 0 & -1 & 0 & 0 \\ 0 & 0 & -1 & 0 & 0 \end{bmatrix}, \quad C_2 = C_1^T,$$

$$C_3 = \frac{1}{16} \begin{bmatrix} -1 & 0 & 0 & 0 & 0 \\ 0 & -1 & -1 & 0 & 0 \\ 0 & -1 & 8 & -1 & 0 \\ 0 & 0 & -1 & -1 & 0 \\ 0 & 0 & 0 & 0 & -1 \end{bmatrix},$$

$$C_4 = \frac{1}{16} \begin{bmatrix} 0 & 0 & 0 & 0 & -1 \\ 0 & 0 & -1 & -1 & 0 \\ 0 & -1 & 8 & -1 & 0 \\ 0 & -1 & -1 & 0 & 0 \\ -1 & 0 & 0 & 0 & 0 \end{bmatrix},$$

$$C_5 = \frac{1}{56} \begin{bmatrix} -1 & -1 & -1 & -1 & -1 \\ -1 & -1 & -2 & -1 & -1 \\ -1 & -2 & 28 & -2 & -1 \\ -1 & -1 & -2 & -1 & -1 \\ -1 & -1 & -1 & -1 & -1 \end{bmatrix}. \quad (12)$$

#### 4. Experimental results

We have conducted several large-scale outdoor experiments to evaluate the stability and capability of the proposed approach. In Fig. 4, we show a scene of interest along with a small inset indicating the road surface distress. The scene is a public road within our campus with minimal traffic intervention. The area of interest contains fine geometric details in the form of small cracks extending to large alligator cracks up to the size of 10 cm in length and width. Our main focus is to accurately and precisely reconstruct and represent details. We note from our experience that inspection of small-sized cracks whose depth and width are in the order of a few millimeters are difficult to capture using our prototype. We believe using multiple or high-speed laser sensors could be a potential solution to generate denser point clouds and higher resolution models. However, we would like to emphasize that the surface reconstruction methods, illustrated in this paper are still effective irrespective of the type and number of sensors deployed in the data acquisition system.

Of the several experiments conducted we have chosen one particular case to express the experience gained in the effort. Fig. 5 shows the trajectory driven for this particular experiment. The measurement van ran a course of 419 m at speeds of 5–10 mph. For visual ease and understanding, we have used a georeferenced satellite image and integrated the 3D motion trajectory coordinates from GPS measurements into the figure. During the data acquisition process, a total of 1291 GPS points, 8840 scanner scans, and 2543 images have been collected. The distance between two successive range scans along the profiling directions varies

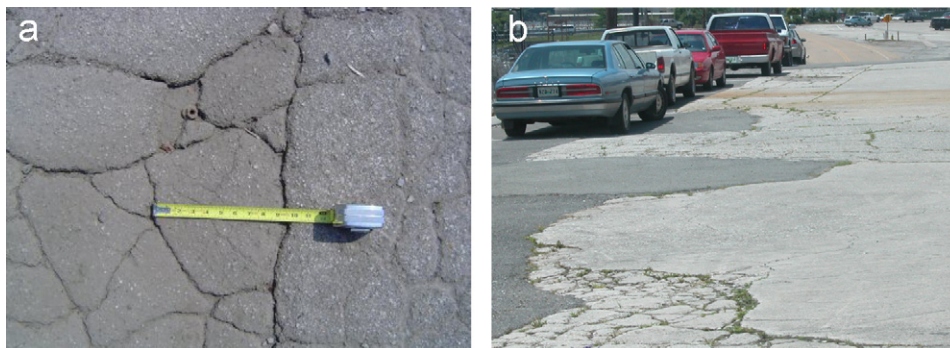


Fig. 4. Road surface of interest with a small section of distress shown enlarged.

with the van velocity from half a centimeter to a few centimeters, typically 3–6 cm at the slow driving speeds for this experiment. The large data has been analyzed and divided into 16 smaller surface patches of interest for further processing. Choosing smaller patches saves computational time and effort since even these smaller patches require 12 megabytes of memory.

From the 419-m stretch, we have selected a small patch containing distress information to present the capability of the proposed post processing algorithms in Fig. 6. This surface patch covers a 90-m long road stretch with a width of 8 m. The points indicative of the road surface alone have been segmented from original registered point cloud using the profile segmentation method previously described. Surface points are physically centered along the scanning

axis with a lower  $z$ -value (i.e. the threshold value is set as 6.3 cm from the ground level). Fig. 6 shows a close view of the segmented result in point cloud format with gray points belonging to different objects. After the profile segmentation, we execute the coarse surface reconstruction scheme from which the areas with distress information can be identified.

A smaller patch that contains distress information is selected from the long stretch in Fig. 6 and is used for detailed reconstruction. The patch covers a 10-m long and 3.6-m wide road surface as shown in Fig. 7, which also shows the results of the two-stage detail-preserving reconstruction. In this example, 26,310 points are included in the original coarse model and 50,074 triangles are generated using 2D Delaunay triangulation. We observe that the mesh points are irregularly distributed and not sampled uniformly. Fig. 7(a) shows the original model and Fig. 7(b) shows the improved triangular interpolation, which preserves topological and geometric details. The interpolated result has 275,340 points and 548,872 triangles. The underlying 2D grid projection has a structured quadrilateral topology in which each rectangular cell has a size of  $1\text{ cm} \times 3\text{ cm}$ . However, as expected the result has imperfections from Gaussian and impulse noise amplified by interpolation as distress features. We remove such artifacts using the regularized smoothing algorithm as the second stage of surface reconstruction. The regularization parameters used in our implementation are  $\lambda_C = 50$ ,

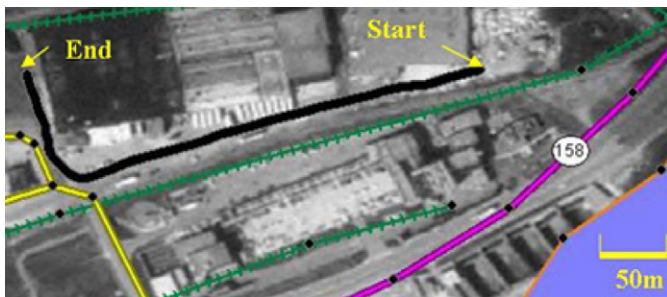


Fig. 5. Trajectory of our scanning system at the scene of interest within our campus visualized on a geo-referenced satellite image.

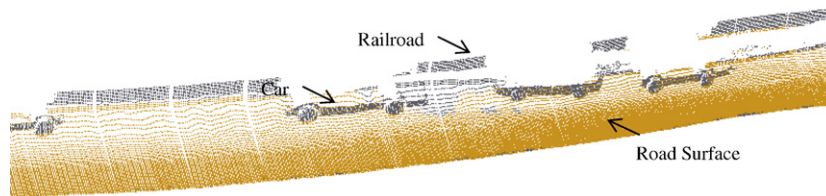


Fig. 6. Reconstructed point cloud with highlighted points indicating road surface points segmented and separated from the other objects such as cars, railroads seen in the original raw data.

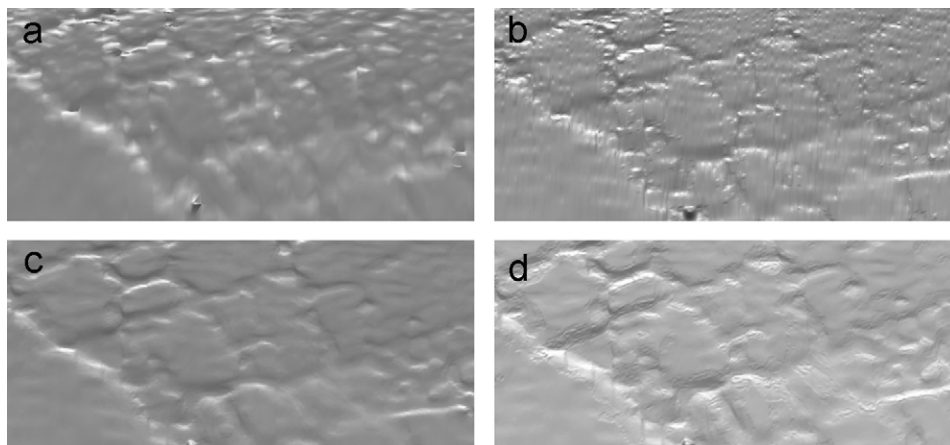


Fig. 7. Two-stage detail surface reconstruction. (a) original model; (b) interpolated model; (c) conventional median filtered result ( $9 \times 9$ ); (d) adaptive regularized smoothing result.

$\lambda_M = 30$ ,  $\beta = 1/\lambda_M$  and  $\varepsilon_{\min} = 0.01$ , respectively. The algorithm converges after five iterations. To emphasize the effect of using a regularized smoothing method, we compare the result with a result obtained with a conventional median filter in Fig. 7(c). We observe that the result from the regularized algorithm which is shown in Fig. 7(d) is able to effectively remove noise while preserving the geometric details of interest.

Now we summarize the whole approach starting from the data acquisition to detailed surface reconstruction in Fig. 8. We show the bird's eye view of the scanned area as a registered point cloud. Since the original range data has over 3 million points, we have sub-sampled with spacing between successive scans being 12–24 cm. From the large point cloud data, we have selected sixteen smaller patches with each patch covering a road corridor that is nearly 200-m long and 4-m wide. A small patch indicated as 'A' is selected for further processing. Only the road surface is segmented from the point cloud 'A' ignoring objects in the environment that are not our interest. The patch marked

'B' is the segmentation result shown right below patch 'A'. This segmented patch is further divided into smaller patches and a small segment marked 'C' is selected and then interpolated using cubic splines and denoised using median filter. The transverse resolution after interpolation and denoising is 1 cm and the distance between successive profile scans is 3–6 cm. We start seeing the alligator cracks on this coarse surface model 'C'. Those interest points belonging to cracks are marked and then reconstructed in detail. The result has an underlying grid with cell size as small as  $1 \times 3$  cm. From the final detailed model marked 'D' the geometry and shape of cracks are easily observed. Road distress information such as mean depth and width of cracks can now be easily computed from those detailed 3D models.

## 5. Conclusions and future work

In summary, we have demonstrated a mobile mapping system acquiring depth, GPS, and IMU data that are

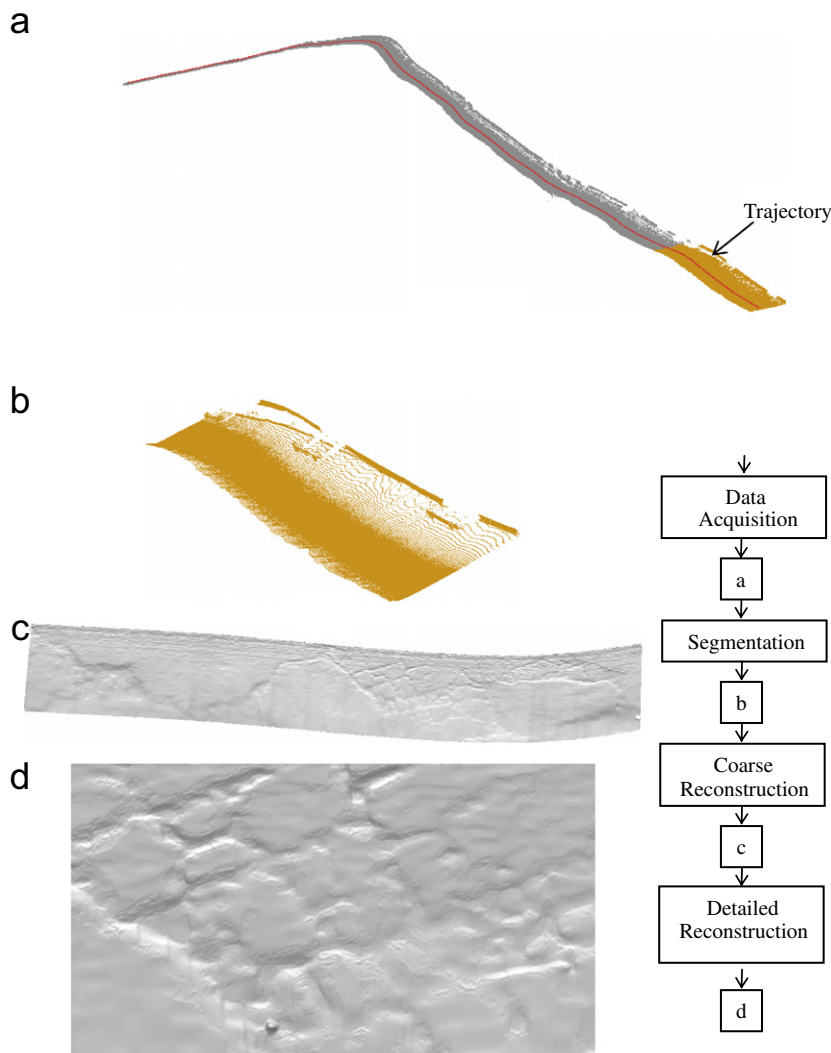


Fig. 8. The proposed approach for reconstructing surface models.

automatically fused to generate 3D models of road surfaces. After processing the acquired data using the algorithms explained in this paper, 3D surface geometric models were created and visualized. The entire procedure requires minimal human intervention in tuning some implementation parameters and selecting areas of interest based on previous experience. The output 3D models show fine geometric details of cracks that are only a few centimeters wide along with the depth information. These models together with higher resolution 2D texture information can be integrated for archiving and analyzing road distress. The surface reconstruction algorithms have also proved to be effective in processing scattered and noisy sampled 3D range data. The reconstructed noise compensated geometry and topology preserving sharp features indicating alligator cracks along with the depth information as a measure of severity is a significant improvement over the commercial systems. Our future efforts will target the development of an efficient strategy to store and visualize large-scale road surfaces employing, for example, a multi-resolution representation at different levels of detail.

### Acknowledgments

This work was supported by the DOE University Research Program in Robotics under Grant DOE-DEFG02-86NE37968 and by the DOD/RDECOM/NAC/ARC Program, R01-1344-18. The authors would also like to thank Doug Warren for helping with the instrumentation of our mobile mapping system.

### References

- [1] Standard practice for quantifying cracks in asphalt pavement surface—AASHTO Designation PP44-01. American Association of State Highway and Transportation Officials, Washington, DC, April 2001.
- [2] Pathview, Pathway Services, Inc. <<http://www.pathwayservices.com>>.
- [3] Automatic Road Analyzer (ARAN), Roadware Group, Inc., <<http://www.roadware.com/aran.htm>>.
- [4] Digital Imaging System, International Cybernetics Corporation, <<http://www.internationalcybernetics.com/imagingvehicle.htm>>.
- [5] Schwarz KP, Martell HE, El-Sheimy N, Li R, Chapman MA, Cosandier D. VIASAT—a mobile highway survey system of high accuracy. In: Proceedings of the IEEE vehicle navigation and information systems conference (VNIS'93), 1993. p. 476–81.
- [6] GeoVAN, GeoSpan Corporation, <<http://www.geospan.com>>.
- [7] Meignen D, Bernadet M, Briand H, One application of neural networks for detection of defects using video data bases: identification of road distresses. In: Proceedings of the eighth international workshop on database and expert systems applications (DEXA '97), 1997. p. 459–64.
- [8] He G. Design and application of the GPS vision mobile mapping system. In: Proceedings of ISPRS commission II symposium on integrated systems for spatial data, vol. XXXIV, part 2, 2002. p. 163–8.
- [9] Gontran H, Skaloud J, Gillieron PY, A mobile mapping system for road data capture via a single camera. In: Proceedings of sixth optical 3D measurement techniques, 2003.
- [10] Cheng HD, Chen JR, Glazier C, Hu YG. Novel approach to pavement cracking detection based on fuzzy set theory. *J Comput Civil Eng* 1999;13(4):270–80.
- [11] Mcghee KH. Automated pavement distress collection techniques—a synthesis of highway practice. Report for national cooperative highway research program (synthesis 334), transportation research board of the national academies, 2004.
- [12] DistressVIEW, GIE Technologies Inc., <<http://www.gietech.com/LVS.htm#Roughness>>.
- [13] Javidi B, Kim D, Kishk S. A laser-based 3D data acquisition system for the analysis of pavement distress and roughness. Technical Report, report No. HR 04-300, Connecticut Department of Transportation, the University of Connecticut, November 2004.
- [14] Laurent J, Talbot M, Doucent M, Road surface inspection using laser scanners adapted for the high precision measurements of large flat surfaces. In: Proceedings of the international conference on recent advances in 3-D digital imaging and modeling (3DIM '97), 1997. p. 303.
- [15] Bursanescu L, Blais F. Automated pavement distress data collection and analysis: a 3-D approach. In: Proceedings of the international conference on recent advances in 3-D digital imaging and modeling, 1997. p. 311–7.
- [16] Abuhadrous I, Ammoun IS, Nashashibi F, Goulette F, Laurgeau C. Digitizing and 3D modeling of urban environments and roads using vehicle-borne laser scanner system. In: Proceedings of RSJ, international conference on intelligent robots and systems (IROS'2004), vol. 1(28), 2004. p. 76–81.
- [17] Tao CV. Mobile mapping technology for road network data acquisition. *J Geospatial Eng* 2000;2(2):1–14.
- [18] Yu SJ, Digitizing and 3D Modeling of road surface using an integrated multisensory approach. Report of the project in lieu of Masters Thesis, University of Tennessee, December 2005.
- [19] Manandhar D, Shibasaki R. Feature extraction from range data. In: Proceedings of the 22nd Asian conference on remote sensing (ACRS), 2001.
- [20] Zhao H, Shibasaki R. A vehicle-borne urban 3-D acquisition system using single-row laser range scanners. *IEEE Trans SMC* 2003; 33(4):658–66.
- [21] Zhao H, Shibasaki R. Update a digital geographic database using vehicle-borne laser scanners and line cameras. *Photogramm Eng Remote Sens* 2005;71(4):415–24.
- [22] Grinstead B, Koschan A, Abidi M. Hybrid self localization for a mobile robotic platform in indoor and outdoor environments. *Trans Am Nucl Soc* 2005;92:52–3.
- [23] Früh C, Zakhor A. Data processing algorithms for generating textured 3D building façade meshes from laser scans and camera images. In: Proceedings of the first international symposium on 3D data processing visualization and transmission (3DPVT'02), 2002. p. 834–47.
- [24] Mann S, Charles L, Michael L, Meyers D, Painter J, DeRose T, et al. A survey of parametric scattered data fitting using triangular interpolants. In: Hagen H, editor. Curve and surface design. Geometric design publications. Philadelphia: SLAM; 1992. p. 145–72.
- [25] Herron G. Smooth closed surfaces with discrete triangular interpolants. *Comput Aid Geometry Des* 1985;2:297–306.
- [26] Sinha SS, Schunck BG. A two-stage algorithm for discontinuity-preserving surface reconstruction. *IEEE Trans PAMI* 1992(14): 136–55.
- [27] Bovik AC, Huang TS, Munson DC. The effect of median filtering on edge estimation and detection. *IEEE Trans PAMI* 1987;9: 181–94.
- [28] Clough R, Tocher J. Finite element stiffness matrices for analysis of plates in bending. Proceedings of conference on matrix methods in structural analysis, 1965.
- [29] Foley TA, Opitz K. Hybrid cubic Bézier triangles patches. In: Lyche T, Schumaker L, editors. Mathematical methods for computer aided

- geometric design. 2nd ed. New York: Academic Press; 1992. p. 275–86.
- [30] Mann S. Cubic precision Clough–Tocher interpolation. *Comput Aid Geom Des* 1999(16):285–8.
- [31] Saaban A, Piah ARM, Majid AA, Chang LHT; G1 scattered data interpolation with minimized sum of squares of principal curvatures. In: Proceedings of the international conference on computer graphics, imaging and visualization (CGIV'05), 2005. p. 385–90.
- [32] Shin JH, Sun Y, Joung WC, Paik JK, Abidi MA. Adaptive regularized noise smoothing of dense range image using directional Laplacian operators. In: Proceedings of SPIE, three-dimensional image capture and applications IV, vol. 4298, 2001. p. 119–26.